Locating Events Using Time Reversal and Deconvolution: Experimental Application and Analysis

**Johannes Douma · Ernst Niederleithinger ·
Roel Snieder**

Abstract Time reversal techniques are used in ocean acoustics, medical imaging, seismology, and non-destructive evaluation to backpropagate recorded signals to the source of origin. We demonstrate experimentally a technique which improves the temporal focus achieved at the source location by utilizing deconvolution. One experiment consists of propagating a signal from a transducer within a concrete block to a single receiver on the surface, and then applying time reversal or deconvolution to focus the energy back at the source location. Another two experiments are run to study the robust nature of deconvolution by investigating the effect of changing the stabilization constant used in the deconvolution and the impact multiple sources have upon deconvolutions' focusing abilities. The results show that we are able to generate an improved temporal focus at the source transducer using deconvolution while maintaining the robust nature of time reversal. Additionally, deconvolution's costs are negligible due to it being a preprocessing step to the recorded data. The technique can be applied for detailed investigation of the source mechanisms (e.g. cracks) but also for monitoring purposes.

Keywords Time reversal · Deconvolution · Concrete · Acoustic emission

J. Douma · R. Snieder
Center for Wave Phenomena,
Colorado School of Mines, Golden, CO, USA
e-mail: jdouma@cimarex.com

R. Snieder
e-mail: rsnieder@mines.edu

E. Niederleithinger (✉)
BAM Federal Institute for Materials Research and Testing,
Berlin, Germany
e-mail: ernst.niederleithinger@bam.de

1 Introduction

Several methods are used to evaluate acoustic signals generated by events in media such as water, rocks, metals or concrete. Most of them are summarized as acoustic emission methods (AE), which are used to localize and characterize the point of origin of the events. Sophisticated methods have been developed in seismology to localize and characterize earthquakes. Time reversal (TR) has been a topic of much research in acoustics due to its robust nature and ability to compress the measured scattered waveforms back at the source point in both space and time [1–4]. This has led to TR being applied in a wide variety of fields such as medicine, communication, ocean acoustics, seismology or nondestructive evaluation. However, continued work is being done to improve TR's ability to focus energy. Some newly developed techniques use an array of input transducers, measure the wave field with an array near the desired focal spot, and then optimize the spatial and temporal focusing [5–13]. Other methods use an array of input transducers and optimize the temporal focusing at an output transducer [14–18].

In this paper, we present evaluation experiments to compare conventional time reversal to an improved variant which uses deconvolution (DC). We explore the application of DC, which is a primitive though robust version of the inverse filter [5,9], to calculate the optimal signal for backpropagation. The ultrasound experiments are performed on a concrete block which has sources embedded within. Instead of using a large array of receivers, the experiments use only a single receiver to record the scattered waveforms. TR or DC is then applied to the measured scattered waveforms to calculate the TR and DC signal. The calculated signals are then backpropagated from a transducer on the surface of the block into the medium and recorded at the original source location transducer. By this experiment, we are able to explore and

compare the capabilities of TR and DC to focus the measured waveforms at a point in both space and time. We show that DC significantly improves the temporal focus compared with TR. We also run two different experiments to study the robust nature of deconvolution by investigating the effect of changing the stabilization constant used in the deconvolution and the impact multiple sources have upon deconvolutions' focusing abilities.

We have shown previously that deconvolution improves temporal focusing [19]. It was then shown by Douma et al. [20] and Douma and Snieder [21] that improved temporal focusing leads to improved spatial focusing as well for both the acoustic and elastic case. Douma et al. [20], Douma and Snieder [21] and Ulrich et al. [19] only used a single source within their experiments and numerical studies. However, within the earth or concrete, multiple fractures may be generated within the time window being recorded. Therefore, the goal of this paper is evaluate the robust nature and focusing capabilities of deconvolution when multiplied source wave fields are generated within a concrete block. Due to deconvolution allowing one to focus an arbitrary source function a source location [19], one could potentially use deconvolution to improve the characterization of the earth or concrete through virtual sources [23–27].

2 Deconvolution Theory

Time reversal (TR) is a process used to compress the measured scattered waveforms at a point in both space and time to ideally a Dirac delta function $\delta(t)$. It uses the recorded impulse response which can be represented by a Green function G_{AB} that accounts for the wave propagation between two points A and B. TR then simply reverses the signal in time and propagates it back from the receiver location into the same medium. By doing so, one expects the energy to focus at the source location. The TR process can be represented by the following equation,

$$\int_{-\infty}^{\infty} G_{AB}(\tau) G_{AB}(\tau - t) d\tau = \delta(t), \tag{1}$$

where reciprocity has been used to replace the Green's function G_{BA} with G_{AB}. According to Eq. 1, the TR process, which is equivalent to the autocorrelation of $G_{AB}(t)$, should ideally lead to equal a delta function. In practice, however, one cannot truly recreate a Dirac delta function focus due to one or more conditions, necessary to satisfy Eq. 1, not upholding. In order for it to work perfectly, one must record for infinite time, Green's functions are assumed to have a flat, infinite bandwidth, the medium is not attenuative, and one must have full coverage of the wavefield at a surface surrounding the points A & B. These requirements are not

upheld during an experiment. This led us to explore the application of deconvolution.

We can rewrite Eq. 1 in a more generalized form (using a convolution notation, rather than the integral form) as

$$F(t) = g(t) \star R(t) \approx \delta(t), \tag{2}$$

where $\star$ denotes convolution, $F(t)$ is the focal signal or source reconstruction, $R(t) = G_{AB}(t) \star S(t)$ is the recorded signal measured at the receiver location B from the initial source propagation where $S(t)$ represent the source as a function of time, and $g(t)$ is the signal necessary to be back propagated for focusing. We are able to go from Eqs. 1 to 2 because we only investigate signals between the two points A and B, and remove the Green function notation to indicate we do not have infinite bandwidth. Thus, we remove some of the unrealistic conditions that are required for Eq. 1 to hold. For a TR process, the signal for backpropagation is purely the time reversed recorded signal: $g(t) = R(-t)$. Our goal is to calculate the optimal signal $g(t)$ such that the focal signal $F(t)$ approximately equals a Dirac delta function $\delta(t)$.

Deconvolution equates to inverse filtering by transforming to the frequency domain, thus Eq. (2) becomes

$$F(\omega) = g(\omega) G(\omega) S(\omega) \approx 1. \tag{3}$$

Equation (3) is used to solve for $g(\omega)$,

$$g(\omega) = \frac{1}{G(\omega) S(\omega)} = \frac{G(\omega)^* S(\omega)^*}{|G(\omega) S(\omega)|^2}, \tag{4}$$

where $*$ denotes complex conjugation. Equation 4 is, however, unrealistic for experimental use in the event that there is a limited bandwidth, significant background noise, or more specifically, if $R(\omega) = 0$ at any frequency. To avoid the associated singularity, we add a constant to the denominator of the last term of Eq. 4 to ensure that we never divide by 0, hence Eq. 4 becomes,

$$g(\omega) = \frac{G(\omega)^* S(\omega)^*}{|G(\omega) S(\omega)|^2 + \epsilon}, \tag{5}$$

where ϵ is a constant related to the original received signal as

$$\epsilon = \gamma \ \text{mean} \left(|G(\omega) S(\omega)|^2 \right). \tag{6}$$

The quantity γ, which is sometimes referred to as the waterlevel parameter [22], is a constant chosen to optimally reduce the effect of noise introduced through the DC procedure. This quantity may equal any positive number where deconvolution could fail due to noise. Here we use $\gamma = 0.9$ for all experiments. The value 0.9 was chosen based on optimizing the focus energy in a process similar to that developed by Clayton and Wiggins [22]. Equation 5 gives the solution for $g(\omega)$. One only has to inverse Fourier transform this result to retrieve the "optimal" DC signal in the time domain to be

backpropagated such that one gets a approximate Dirac delta function focus.

3 Experimental Set Up

A laboratory experiment was created and run in the Civil Engineering lab of Colorado School of Mines. A $30 \times 30 \times 37\,cm^3$ concrete block was cast from 72 kg Quickcrete mix (No. 1101, max aggregate grain size <4 mm), with about 60 liters water and 5 kg of additional gravel (5–15 mm grain size). The concrete used has a nominal compressive strength of 27.9 MPa after curing for 28 days in accordance to ASTM C39/ASTM 387. The block contains only minimal reinforcement as shown in Fig. 1a. Three ultrasonic piezo transducers (type Acsys SO807, center frequency 60 kHz, labeled 'ES' in Fig. 1) were attached to the reinforcement in order to cast them within the concrete block. These sources (transducers) are visible in Fig. 1a. These sources were oriented differently in order to generate more complex waveforms and to study the effect of varying source orientation. Source 3 was oriented perpendicular to the other two sources. Broadband Acsys sensors type 1803 (center frequency about 100 kHz, labeled 'PT' in Fig. 1) were used as external transducers. They are piezo-based and feature a spring-loaded 2 mm diameter ceramic tip for contact to the concrete. These transducers are most sensitive in the direction perpendicular to the surface it is attached to. The transmitted signal is generated by a custom made rectangular signal generator/amplifier (BAM US in Fig. 1). It is triggered by a TTL impulse which is issued by our data acquisition device (National Instruments model 6366). The recorded signals at the external sensor are first high pass filtered at a frequency of 1 kHz and amplified by a Stanford Research low noise preamplifier (SR 566) before being digitized and recorded. This was necessary to remove low frequency noise present in our data. The workflow and set up used for acquiring the data is shown in Fig. 1b. Additionally, in order to reduce noise, we have used time averaging by stacking over 144 runs.

For backpropagation, the setup is reversed. The BAM US device is removed. The transmitter signal generator is replaced by the digital/analog converter integrated in the data acquisition device, sending the computed, time reversed/deconvolved waveforms to the external sensor. The embedded sensor is used as receiver, again using the preamplifier before AD conversion and recording. This reversed set up is shown in Fig. 1c. We have used a sampling frequency of 2 MHz and 20,000 samples per trace (10 ms recording time). A 4,000 sample (2 ms) pre-trigger interval was set. The reason a longer pre-trigger time was used is because it was shown by Ulrich et al. [19] that with a longer pre-trigger time, we were able to improve the focus for deconvolution. Amplitude resolution is 16 bit. True zero time of the transmitter could be
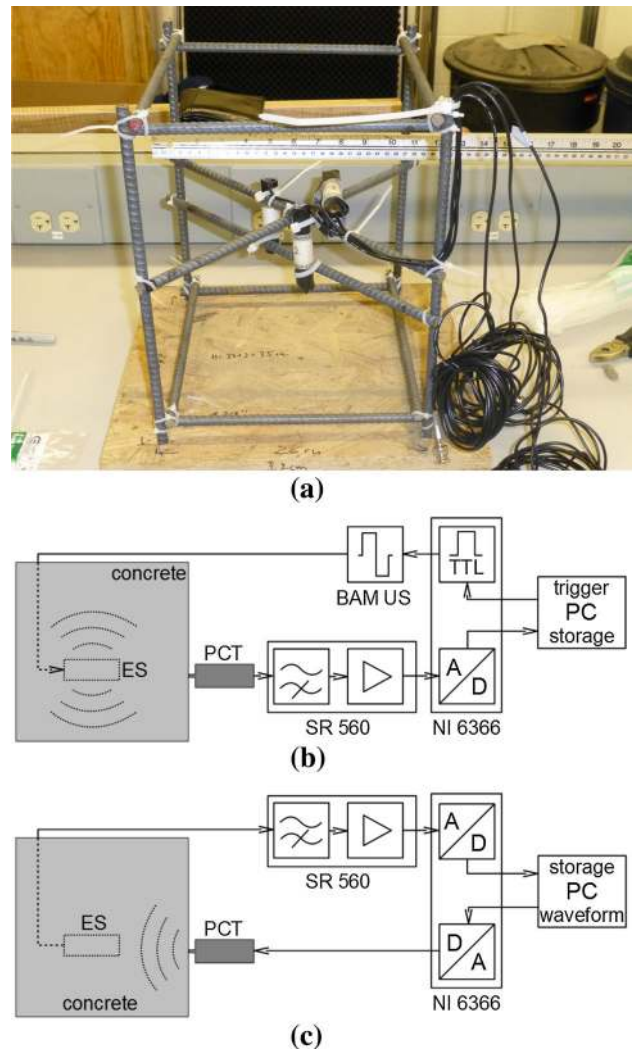

Fig. 1 Figures and diagrams indicating experimental set up and workflows used during acquisition and backpropagation. Note, the diagrams indicating the workflows are meant to show the tools used during acquisition and backpropagation and do not accurately describe the interior of the concrete for every experiment in this paper. **a** Source set up and reinforcement to be placed within the concrete block, **b** acquisition workflow, **c** backpropagation workflow

identified by electromagnetic crosstalk between transmitter and receiver cables, generating a small but easy to recognize impulse in the receiver data. The laboratory contained other noise due to multiple experiments being run simultaneously. Due to a high noise lab environment and a lack of a power amplifier for the backpropagated transmitter signal, we apply an additional 2 kHz high-pass Butterworth filter on all data.

In order to test the stability of deconvolution for different values of the regularization parameter γ, we run the exact same experiment as for a single source described above and shown in Fig. 1b. Once the signal was recorded, we applied DC multiple times with different gamma values in order to

generate the different signals to be backpropagated. We then ran the same workflow as shown in Fig. 1c for each DC signal separate, recording the focused wavefield at the source location each time.

For multiple sources, we executed the workflow described above and shown in Fig. 1b three times (once for every source). This was necessary because we did not have the equipment capabilities in this laboratory to generate a source function at all three source locations at different onset times. We recorded these three generated wavefields separately and then superimposed them. Due to the experiment being run separately three times, each recorded signal was normalized independently. This caused our recorded signals for all three sources to vary between amplitudes of −1 and 1. Thus, it destroyed the relative amplitude variation one would expect for three different sources at different locations and orientations. Once superimposed, TR or DC was applied and we carried out the same back propagation workflow as shown in Fig. 1c. During the backpropagation, one restores the relative amplitudes in the focus achieved because of reciprocity.

4 Data Analysis

4.1 Single Source Experiment

The purpose of this experiment is to study the capabilities of TR and DC to focus the measured waveforms at a point in time. The experiment began with propagating a defined 60 kHz source function from the embedded source towards the external receiver. The receiver's direction of measurement was perpendicular to the direction of source emission. Once our wave field was recorded at the single receiver, TR or DC was applied to calculate the back propagating signals.

For a single source, deconvolution ideally achieves an improved temporal focus. This is due to there being a single term in the denominator as shown in Eq. 5, which leads to the following,

$$g(\omega)G(\omega) \approx \frac{G(\omega)G^*(\omega)S^*(\omega)}{|G(\omega)S(\omega)|^2 + \epsilon} \approx \frac{1}{S(\omega)}, \tag{7}$$

where $G(\omega)$ represents the Green's function describing the propagation between source and receiver, $S(\omega)$ represent the source function in the frequency domain, and $g(\omega)$ the signal we are trying to solve for with deconvolution. Equation 7 should approach $1/S(\omega)$ as ϵ approaches 0. Therefore, the focus achieved using deconvolution approaches an optimal reconstruction of the inverse of the source function and not necessarily a Dirac delta function. When the source function is a delta function, $S(\omega)$ is constant, this leads to a delta function at the focal point.
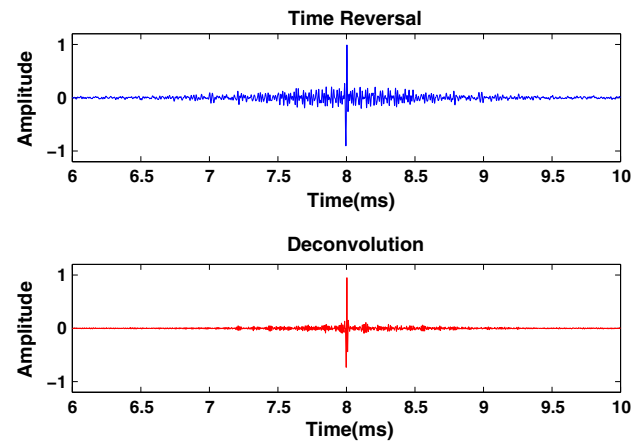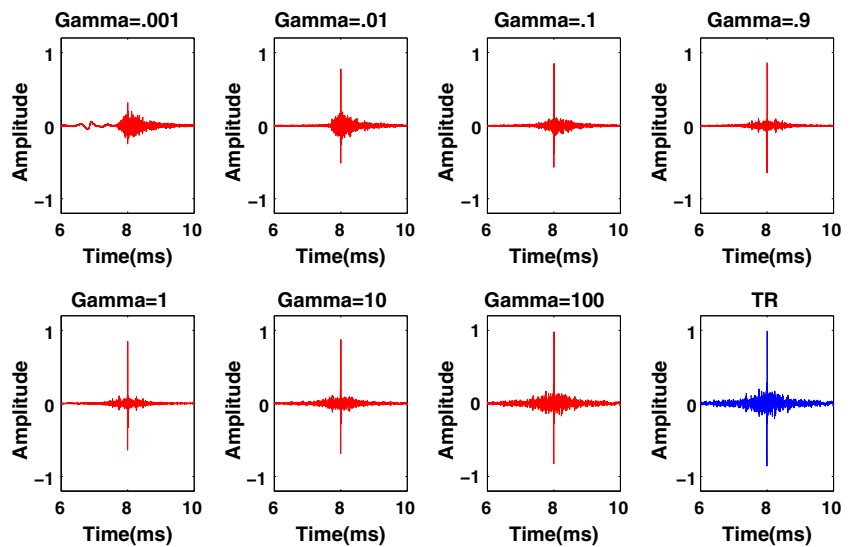

Fig. 2 Normalized temporal focus measured at the embedded source location using (*top panel*) time reversal, and (*bottom panel*) deconvolution for a single source and single receiver set up

The DC and TR signals were then backpropagated from the transducer on the surface of the block into the same medium and recorded at the original source location transducer. Figure 2 show the refocused waves recorded at the source location where Fig. 2a is the temporal focus achieved using TR while Fig. 2b represents the temporal focus achieved using the DC calculated signal. The temporal focus achieved using TR has significant side-lobes away from the time of focus; the temporal focus achieved using DC has suppressed most of these side-lobes and was able to produce a better focus. In order to quantify this improvement, we calculate the amount of energy in a 0.02 ms window around the time of focus compared to the total energy of the signal. The temporal focus achieved using TR only had 41 % of the total energy within this window while DC's temporal focus had 80 % of the total energy within this window. Thus, DC is able to generate a significantly better temporal focus than TR. Our source function used wasn't a Dirac delta function but deconvolution still improved the focus significantly as it improved the reconstruction of our source function. Once we had shown that deconvolution was able to improve the focus at a point in time, we continued our experimental studies to investigate the robust nature of deconvolution.

4.2 Regularizing the Deconvolution

The purpose of this experiment was to study the robust nature of DC by changing the location of the receiver and investigating the effect of regularizing the deconvolution through the parameter ϵ used in Eq. 5. This experiment started the same way as our previous single source experiment. We first propagated a defined 60 kHz source function from the embedded source towards the external receiver. For this experiment, the receiver's direction of measurement was parallel to the direction of source emission. The recorded signal was then

Fig. 3 Normalized temporal focus measured at the embedded source location using different values for γ in the deconvolution (shown in *red*) and time reversal (shown in *blue*) (Color figure online)
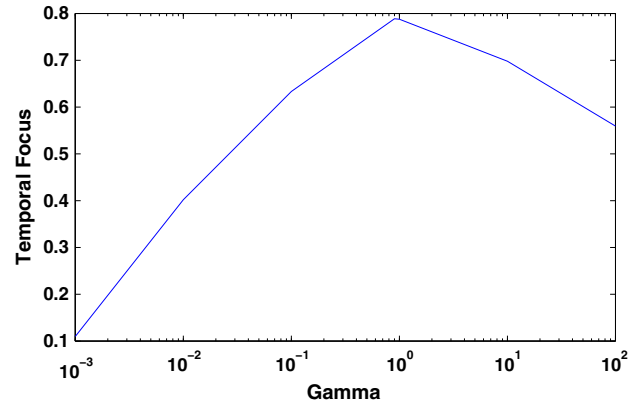

Fig. 4 The temporal focus, defined as the amount of energy in a 0.02 ms window around the time of focus compared to the total energy of the signal, as function of γ. High temporal focus indicates most of the energy is compressed at the time of focus

deconvolved using various values of γ which was the constant scalar number used to characterize the regularization term ϵ defined in Eq. 6. These calculated deconvolved signals were propagated back into the medium from the receiver location and recorded at the source transducer.

Theoretically, we would expect the focused wavefield to contain significant amount of noise at low γ values. As γ increases, the temporal focus is expected to improve because we reduce the effect of noise and force our signal to generate a better approximate Dirac delta function focus. However, if γ becomes too large, one approaches the temporal focus achieved using TR. This can be seen as follows: For time reversal, $g(t) = R(-t)$, therefore, $g(\omega) = R^*(\omega)$. If γ is large, ϵ becomes large in the sense that $\epsilon >> |R(\omega)|^2$, and Eq. 5 reduces to

$$g(\omega) \approx \frac{1}{\epsilon} G(\omega)^* S(\omega)^* = \frac{1}{\epsilon} R^*(\omega), \qquad (8)$$

which implies that our deconvolved signal is just a scaled version of the time reversed signal.

Figure 3 shows the normalized focused wavefield at the source location for TR and DC for different values of γ. For this experiment, we quantified the temporal focus the same way as the previous experiment with the identical window size of 0.02 ms used. The optimal DC's temporal focus was 79 % (for a gamma value of 0.9) while TR had a temporal focus of 47 %. We would not expect to see the exact same temporal focusing numbers as in our single source experiment because we changed the direction of displacement we record and the distance between the source and receiver.

Figure 4 highlights the effect of gamma by showing the temporal focus as a function of γ. If γ becomes small, the temporal focus achieved decreases. However, as γ becomes large, the temporal focus approaches TR's temporal focus of 47 %. The experiment showed that the optimal value to be $\gamma = 0.9$. However, even for different γ values, one still achieves some form of a temporal focus as shown in Fig. 3.

4.3 Multi Source Experiment

The purpose of this experiment was to study the effect of multiple sources when using deconvolution. We began by emitting the same 60 kHz source function from different source transducers within the concrete block at different onset times. The experiment was repeated three times to record each source wavefield separately which normalized the recorded signals independently. The employed normalization caused our signals for all three sources to vary between amplitudes of -1 and 1. The three recorded wavefields due to the three sources were then superimposed before TR or DC was applied. Figure 5 shows the superimposed wavefield. Note the complexity of the wavefield due to scattering within
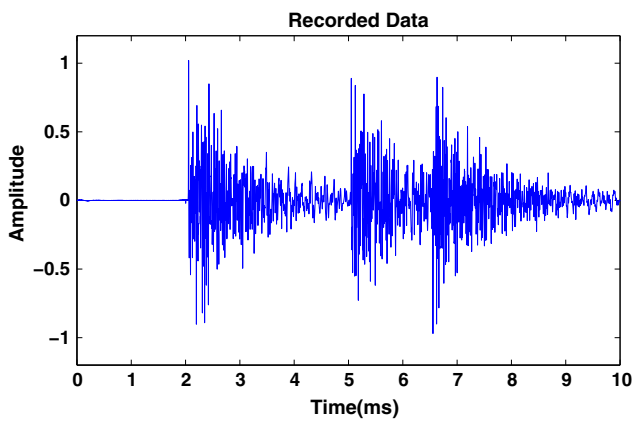
Recorded Data

Fig. 5 Recorded scattered waveforms at the receiver location due to three source wavefields being emitted at different times
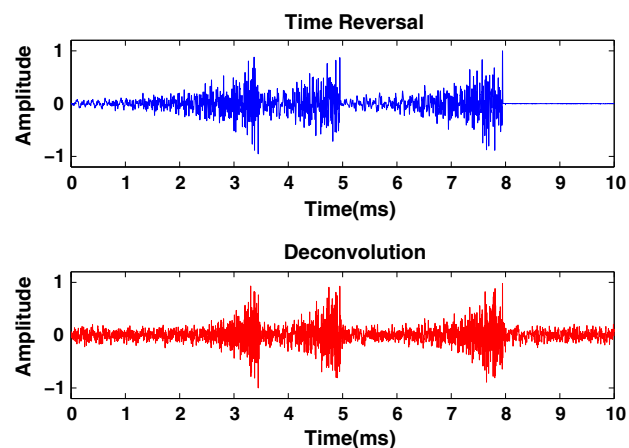
Time Reversal

Deconvolution

Fig. 6 Back propagation signals calculated using Time reversal (*top panel*) and deconvolution (*bottom panel*). These signals are backpropagated into the medium for the multi-source experiment

the concrete sample. Due to the complicated nature of the recorded signal, one can assume that the cross-correlation of each source wave field is negligible:

$$G_i G_j^* \approx 0 \quad \text{for } i \neq j \tag{9}$$

where G_i for $i = 1, 2, 3$ is the Green's function characterizing the source wavefield for sources 1, 2, or 3. Equation 9 is crucial in explaining why deconvolution is stable for multiple sources.

We apply time reversal and deconvolution to the superimposed signal consisting of the three source wavefields to generate our TR and DC signals shown in Fig. 6. Deconvolution's signal differs from time reversal signal in its acausal nature, due to our pre-trigger time, where DC adds information past 8 ms while TR has zero amplitude after 8 ms. Additionally, the three different source wavefields are still clearly visible in the DC signal. Below, we demonstrate why deconvolution is able to focus the wavefield due to multiple source at each source location.

If there are three sources, the recorded signal in the frequency domain is given by

$$R(\omega) = G_1 S_1 + G_2 S_2 + G_3 S_3, \tag{10}$$

where $R(\omega)$ is the recorded signal in the frequency domain, and the subscripts indicate the source transducer used. The inverse signal obtained by deconvolution is given by

$$\begin{aligned} D_t(\omega) &= \frac{1}{G_1 S_1 + G_2 S_2 + G_3 S_3} \\ &= \frac{1}{(G_1 S_1 + G_2 S_2 + G_3 S_3)} \frac{(G_1 S_1 + G_2 S_2 + G_3 S_3)^*}{(G_1 S_1 + G_2 S_2 + G_3 S_3)^*}. \end{aligned} \tag{11}$$

We simplify the above solution and add the regulation term $\epsilon = \gamma \, \text{mean}(|R(\omega)|^2)$ to get,

$$D_t(\omega) = \frac{(G_1 S_1 + G_2 S_2 + G_3 S_3)^*}{|G_1 S_1|^2 + |G_2 S_2|^2 + |G_3 S_3|^2 + \text{Crosstalk} + \epsilon}, \tag{12}$$

where $\text{Crosstalk} = G_1 S_1 G_2^* S_2^* + G_1 S_1 G_3^* S_3^* + G_2 S_2 G_1^* S_1^* + G_2 S_2 G_3^* S_3^* + G_3 S_3 G_1^* S_1^* + G_3 S_3 G_2^* S_2^*$, and $D_t(\omega)$ represents the deconvolved signal when the recorded signal contains three source wavefields.

If we recorded each sources' wavefield separate and applied deconvolution first before the superposition of the wavefields, we would get:

$$D_s(\omega) = \frac{(G_1 S_1)^*}{|G_1 S_1|^2 + \epsilon_1} + \frac{(G_2 S_2)^*}{|G_2 S_2|^2 + \epsilon_2} + \frac{(G_3 S_3)^*}{|G_3 S_3|^2 + \epsilon_3}, \tag{13}$$

where $D_s(\omega)$ represents the deconvolved signal when deconvolution is applied before superposition. One might expect that for a real scenario, where multiple sources are present, deconvolution would break down due to the influence of crosstalk. Because the recorded wavefields generated by each source are extremely complex, as shown in Fig. 5, terms such as $G_1 G_2^*$ are small (Eq. 9). Therefore, the influence of the crosstalk terms is minimal and we can assume it vanishes. This provides us with the following solution that relates $D_s(\omega)$ to $D_t(\omega)$,

$$\begin{aligned} D_s(\omega) &= \frac{(G_1 S_1)^*}{|G_1 S_1|^2 + \epsilon_1} + \frac{(G_2 S_2)^*}{|G_2 S_2|^2 + \epsilon_2} + \frac{(G_3 S_3)^*}{|G_3 S_3|^2 + \epsilon_3} \\ &\approx 3 \frac{(G_1 S_1 + G_2 S_2 + G_3 S_3)^*}{|G_1 S_1|^2 + |G_2 S_2|^2 + |G_3 S_3|^2 + \epsilon} = 3 D_t(\omega), \end{aligned} \tag{14}$$

where we assume $|G_1 S_1| \approx |G_2 S_2| \approx |G_3 S_3|$.

Figure 7 shows that the approximation (14) holds. Figure 7 demonstrates that after normalizing $D_s(t)$ and $D_t(t)$, one can note that there does not seem to be a obvious difference between $D_s(t)$ and $D_t(t)$. Therefore, one may conclude Thus, the crosstalk term may be ignored and deconvo-
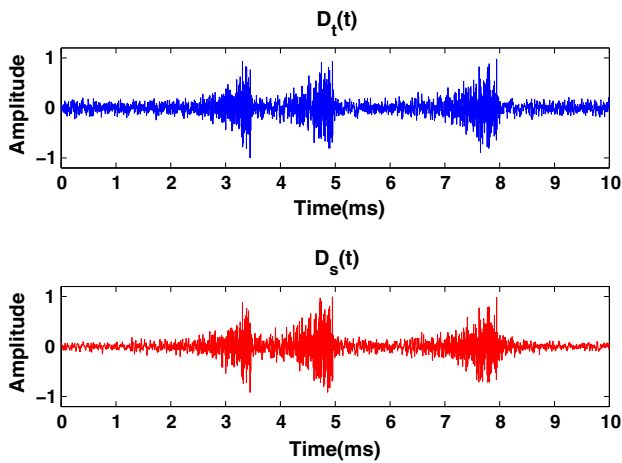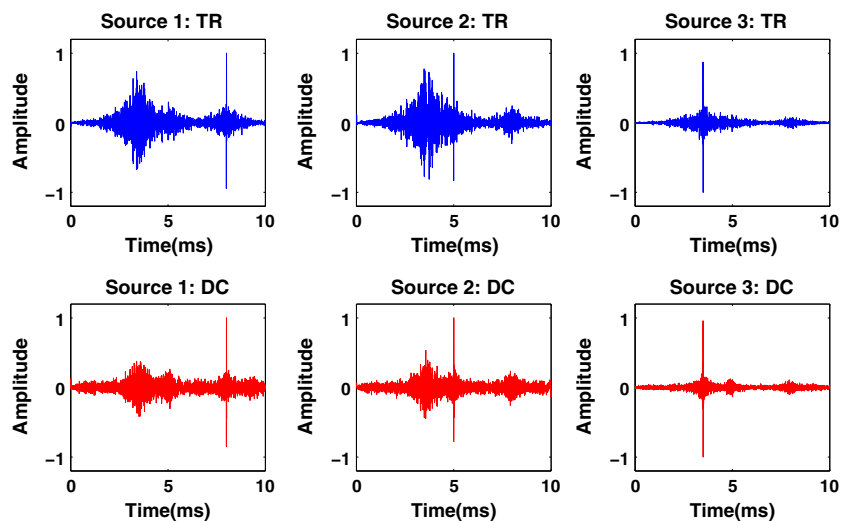
Fig. 7 Comparison of deconvolution signal calculation. *Top panel* shows the DC signal after applying deconvolution to the superposition of the three recorded wavefields $D_t(t)$. *Bottom panel* shows the DC signal after applying deconvolution to the three recorded signals before adding them to each other $D_s(t)$. All signals are normalized

lution is stable and able to focus the wavefield due to multiple sources at each source location. We were able to do this calculation because we recorded each source wavefield separately.

One does not need to have priori knowledge of the source signal in order to apply deconvolution and detect the sources. One can essentially modify the focus to be any arbitrary source function as shown in Ulrich et al. [19]. We have just assumed the source function to be a Dirac delta function for these experiments.

In order to keep the experiment realistic, we back propagated the DC signal which was calculated after the superposition of the three separate wavefields. Figure 6 shows the signals calculated using TR and DC which are propagated back into the medium from the receiver location. We

then used the transducers within the concrete block as our receivers. Figure 8 shows the focused wavefields at each of the three sources for TR, shown in the top panels, versus DC, shown in the bottom panels. For sources 1 and 2, deconvolution compresses the sidelobes substantially better than TR. However, for source 3, deconvolution does not significantly improve the focus compared to time reversal.

The orientation of our sources is an important factor. Sources 1 and 2 were oriented perpendicular to source 3, and as a result the recorded waves excited by source 3 are stronger than those excited by sources 1 and 2. However, as previously stated, we ran each source wavefield propagation separately which normalized the recorded signals independently causing the amplitudes of each recorded source wavefield to vary between amplitudes of -1 and 1. Thus, our superimposed signal shown in Fig. 5 does not show a higher amplitude for the source 3 wavefield. However, when we back propagate our TR and DC wavefield, due to reciprocity, the source 3 wavefield focus will have a higher amplitude. This causes the crosstalk terms to be negligible for the source 3 focus because,

$$|G_3(\omega)| >> |G_1(\omega)| \quad \text{and} \quad |G_3(\omega)| >> |G_2(\omega)|. \quad (15)$$

Under these conditions, Eq. 12 reduces to,

$$D_t(\omega) \approx \frac{(G_3 S_3)^*}{|G_3 S_3|^2 + \epsilon}, \quad (16)$$

which is what we had before.

Figure 8 show that Eq. 15 holds because, for source 3, the focus has significantly higher relative amplitude than the crosstalk terms. For sources 1 and 2, the maximum amplitude of the crosstalk is closer to the maximum amplitude of its focus.

In conclusion, for multiple sources, deconvolution is able to focus the energy at the source location at the correct time. It is arguable whether time reversal or deconvolution is better

Fig. 8 Temporal focus measured at the three embedded source location using (*top panels*) time Reversal's signal, and (*bottom panels*) deconvolution's $D_t(t)$ signal and back propagating it from the transducer on the surface of the concrete sample

in generating a focus. However, the experiment does prove the robust nature of DC in that it does not fail under the condition of multiple sources.

The purpose of using time reversal (TR) and deconvolution (DC) processes is to generate a signal such that it will focus at the source location. One can use this feature of the methods for a range of applications in order to characterize the medium. For example, after the time of focus, the wave field will propagate away from the source location with the characteristic as if it were generated by a source mechanism at the focused event location. This is defined as a "virtual" source. This "virtual" source can then be used to for a wide variety of applications from multiple suppression, to medium characterization [23–27]. Additionally, one can continuously monitor and backpropagate signals to investigate the changes occurring within the medium. Using DC, one can also define the type of source function focus that will occur at the event location. This was shown to work by Ulrich et al. [19]. Therefore, one could determine the frequency of the focused wave field and allow different frequency focuses to occur. One then records the scattered wave field generated by the virtual sources consisting of different frequencies to characterize the medium. Therefore, by using DC, we could potentially improve the characterization of the medium compared with TR. In addition, the amplitude can be varied to study non-linear effects. Finally, another application is the locating of microseismic events and fractures within a medium by using reverse-time imaging [21].

5 Conclusion

We have introduced in an experimental study a simple though robust method for determining the optimal signal for backpropagation such that one gets an improved temporal focus at the source location. Deconvolution was shown to have an optimal regularization parameter, γ, for improved temporal focusing. If one increases γ, the temporal focus approaches that of TR; if one decreases γ, one increases the effect of noise and the temporal focus decreases dramatically. However, Fig. 4 shows that one still attains a temporal focus even for different values of γ. Additionally, deconvolution does not break down when there are multiple source wavefields being propagated. This is due to the influence of the crosstalk terms being minimal for the complicated waveforms generated by scattering in the concrete. Thus, deconvolution has a robust nature comparable to that of time reversal while having the potential to dramatically improve the focus. In conclusion, the simple and robust nature of deconvolution allows it to be implemented as a preprocessing step in order to improve focusing at the source location.

References

1. Parvulescu, A., Clay, C.: Reproducibility of signal transmission in the ocean. Radio Electron. Eng. **29**, 223–228 (1965)
2. Fink, M.: Time reversed acoustics. Phys. Today **50**(3), 34–40 (1997)
3. Anderson, B.E., Griffa, M., Larmat, C., Ulrich, T.J., Johnson, P.A.: Time reversal. Acoust. Today **4**(1), 5–16 (2008)
4. Larmat, C.S., Guyer, R.A., Johnson, P.A.: Time-reversal methods in geophysics. Phys. Today **63**(8), 31–35 (2010)
5. Tanter, M., Thomas, J.-L., Fink, M.: Time reversal and the inverse filter. J. Acoust. Soc. Am. **108**, 223–234 (2000)
6. Tanter, M., Aubry, J.-F., Gerber, J., Thomas, J.-L., Fink, M.: Optimal focusing by spatio-temporal filter. I. Basic principles. J. Acoust. Soc. Am. **110**, 37–47 (2001)
7. Montaldo, G., Tanter, M., Fink, M.: Real time inverse filter focusing through iterative time reversal. J. Acoust. Soc. Am. **115**, 768–775 (2004)
8. Vignon, F., Aubry, J.-F., Saez, A., Tanter, M., Cassereau, D., Montaldo, G., Fink, M.: The Stokes relations linking time reversal and the inverse filter. J. Acoust. Soc. Am. **119**, 1335–1346 (2006)
9. Gallot, T., Catheline, S., Roux, P., Campillo, M.: A passive inverse filter for Green's function retrieval. J. Acoust. Soc. Am. **131**, EL21–EL27 (2011)
10. Bertaix, V., Garson, J., Quieffin, N., Catheline, S., Derosny, J., Fink, M.: Time-reversal breaking of acoustic waves in a cavity. Am. J. Phys. **72**(10), 1308 (2004)
11. Roux, P., Fink, M.: Time reversal in a waveguide: study of the temporal and spatial focusing. J. Acoust. Soc. Am. **107**, 2418–2429 (2000)
12. Aubry, J.-F., Tanter, M., Gerber, J., Thomas, J.-L., Fink, M.: Optimal focusing by spatio-temporal filter. II. Experiments. Application to focusing through absorbing and reverberating media. J. Acoust. Soc. Am. **110**, 48–58 (2001)
13. Jonsson, B.L.G., Gustafsson, M., Weston, V.H., de Hoop, M.V.: Retrofocusing of acoustic wave fields by iterated time reversal. SIAM J. Appl. Math. **64**(6), 1954–1986 (2004)
14. Daniels, R., Heath, R.: Improving on time reversal with MISO pre-coding. In: Proceedings of the Eighth International Symposium of Wireless Personal Communications Conference, Aalborg, Denmark, pp. VI-124–VI-129 (2005)
15. Qiu, R.C., Zhou, C., Guo, N., Zhang, J.Q.: Time reversal with MISO for ultrawideband communications: experimental results. IEEE Antennas Wirel. Propag. Lett. **5**, 1–5 (2006)
16. Blomgren, P., Kyritsi, P., Kim, A., Papanicolaou, G.: Spatial focusing and intersymbol interference on multiple-input-single-output time reversal communication systems. IEEE J. Ocean. Eng. **33**, 341–355 (2008)
17. Zhou, C., Guo, N., Qiu, R.C.: Experimental results on multiple-input single-output (MISO) time reversal for UWB systems in an office environment. In: MILCOM'06 Proceedings of the 2006 IEEE Conference on Military Communications, pp. 1299–1304. IEEE Press, Piscataway, NJ (2006)
18. Zhou, C., Qiu, R.C.: Spatial focusing of time-reversed UWB electromagnetic waves in a hallway environment. In: Proceedings of the Thirty Eighth Symposium on System Theory, pp. 318–322 (2006)
19. Ulrich, T.J., Douma, J., Anderson, B.E., Snieder, R.: Improving spatio-temporal focusing and source reconstruction through deconvolution. Wave Motion (2014). doi:10.1016/j.wavemoti.2014.10.001
20. Douma, J., Snieder, R., Fish, A., Sava, P.: Locating a microseismic event using deconvolution. In: Proceedings of the 83rd Annual International Meeting, Society of Exploration Geophysicists (2013)

21. Douma, J., Snieder, R.: Focusing of elastic waves for microseismic imaging. Geophys. J. Int. 200(1), 390–401 (2015)
22. Clayton, R., Wiggins, R.: Source shape estimation and deconvolution of teleseismic bodywaves. Geophys. J. R. Astron. Soc. **47**, 151–177 (1976)
23. Wapenaar, K., Broggini, F., Snieder, R.: Creating a virtual source inside a medium from reflection data: heuristic derivation and stationary-phase analysis. Geophys. J. Int. **190**, 1020–1024 (2012)
24. Behura, J., Snieder, R.: Virtual Real Source: source signature estimation using seismic interferometry. Geophysics **78**, Q57–Q68 (2013)
25. Mehta, K., Sheiman, J., Snieder, R., Calvert, R.: Strengthening the virtual-source method for time-lapse monitoring. Geophysics **73**, S73–S80 (2008)
26. Snieder, R., Sheiman, J., Calvert, R.: Equivalence of the virtual-source method and wave-field deconvolution in seismic interferometry. Phys. Rev. E **73**, 066620 (2006)
27. Mehta, K., Snieder, R., Calvert, R., Sheiman, J.: Acquisition geometry requirements for generating virtual-source data. Lead. Edge **27**(5), 620–629 (2008)